Journal of Cleaner Production 256 (2020) 120440

Contents lists available at ScienceDirect

Journal of Cleaner Production

journal homepage: www.elsevier.com/locate/jclepro

Remediation of contaminated soil by red mud and paper ash

P. Oprčkal [a], A. Mladenovič [a], N. Zupančič [b], J. Ščančar [c, d], R. Milačič [c, d], V. Zalar Serjun [a, *]

[a] Slovenian National Building and Civil Engineering Institute, Dimičeva 12, 1000, Ljubljana, Slovenia
[b] University of Ljubljana, Faculty of Natural Sciences and Engineering, Department of Geology, Aškerčeva 12, 1000, Ljubljana, Slovenia
[c] Department of Environmental Sciences, Jožef Stefan Institute, Jamova 39, 1000, Ljubljana, Slovenia
[d] Jožef Stefan International Postgraduate School, Jamova 39, 1000, Ljubljana, Slovenia

ARTICLE INFO

Article history:
Received 20 March 2019
Received in revised form
3 December 2019
Accepted 4 February 2020
Available online 7 February 2020

Handling editor: CT Lee

Keywords:
Red mud
Paper ash
Contaminated soil
Potentially toxic elements
Geotechnical composites

ABSTRACT

Remediation of contaminated soil can be performed by using various techniques, which must be adequately tailored for each specific case. The aim of this research is to critically evaluate the potential use of red mud and paper ash and a combination of the two as immobilization additives for the remediation of contaminated soil from one of the most polluted sites in Slovenia. The proposed procedure involves the preparation of geotechnical composites made from contaminated soil and mixed with 25 wt% of immobilization additives and an optimal quantity of water to achieve consistency, at which maximum compaction according to the Proctor Compaction Test procedure can be achieved. The results reveal a positive, time-dependent trend for the immobilization of potentially toxic elements in the composite with paper ash, because of the formation of the new hydration products with potentially toxic elements. In a composite containing only red mud, potentially toxic elements were immobilized by sorption mechanisms with no general time-dependent trends. The composite with a combination of additives demonstrates the remediation characteristics of both red mud and paper ash. Using this approach excavated contaminated soil, red mud and paper ash can be successfully recycled in the proposed composites, which can be beneficially used in situ for rehabilitation of contaminated sites. Nevertheless, mobilization of some potentially toxic elements at high pHs may represent a limiting factor and has to be taken into the consideration when a combination of red mud and paper ash is used as immobilization additive.

© 2020 The Authors. Published by Elsevier Ltd. This is an open access article under the CC BY-NC-ND license (http://creativecommons.org/licenses/by-nc-nd/4.0/).

1. Introduction

The management of contaminated soil poses a great challenge from the perspective of human and ecosystem health, and from that of economic and social development (van Hees et al., 2008). According to data provided by the European Environmental Agency (EEA), there are at least 342,000 sites with contaminated soil in Europe alone (EEA, 2014). In 34.8% of all these cases of soil contamination, potentially toxic elements (PTEs) are the most common type of contaminant (EEA, 2014). Excavated contaminated soil can be categorized into non-hazardous or hazardous waste, and relevant management techniques can be employed according to the waste hierarchy, with landfilling being the least desirable option and recycling the most. Soil recycling and remediation can be regarded as an "R5" recovery operation within the European legislative framework ["…soil cleaning resulting in the recovery of soil and recycling of inorganic construction materials"] (European Commission, 2008). Current remediation procedures aim to eliminate the transfer pathways of PTE from contaminated soil to receptors (humans, animals, and the environment). These procedures include different physical and chemical treatment options, of which immobilization has been recommended by the EU Commission as the Best Available Technique (European Commission, 2006). The selection of an appropriate additive is crucial for successful immobilization. Produced in large quantities, conventional binders as well as recycled waste materials from different industrial processes can be used for the immobilization, for example blast furnace slag and fly ash (Zhou and Haynes, 2010).

Red mud (RM) is a waste material that has the potential to be used for the purpose of immobilization in soil remediation. Approximately 170 Mt of RM—a waste material from alumina production—was generated worldwide in 2015 (Hua et al., 2017), typically deposited in large lagoons or land-based disposal pits. RM can pose a health hazard to the local environment and population

* Corresponding author.
E-mail address: vesna.zalar@zag.si (V. Zalar Serjun).

https://doi.org/10.1016/j.jclepro.2020.120440
0959-6526/© 2020 The Authors. Published by Elsevier Ltd. This is an open access article under the CC BY-NC-ND license (http://creativecommons.org/licenses/by-nc-nd/4.0/).

due to its high alkalinity and high total concentrations of PTEs (Hua et al., 2017). Chemical and physical properties of RM may vary considerably, reflecting its diverse range of sources (Klauber et al., 2011). Cases of successful use of RM for the immobilization of contaminants in soil have been reported (comprehensive literature review presented in Table S1). Main immobilization mechanisms of PTE assigned to the RM amendment are—high sorption capacity, surface complexation, and formation of inner-sphere complexes (Hua et al., 2017; Khairul et al., 2019). Partial neutralization of highly alkaline RM is required to achieve better adsorption capacity and enable its safe use (Pichinelli et al., 2017).

Another alternative recycled material which has potential soil remediation uses is paper ash (PA), a highly alkaline material that contains (latent) hydraulically active phases (Segui et al., 2012). The official data from the European paper and pulp industry reveal that, in the EU, paper mills generate 11 Mt of waste annually, approximately 70% of which represents waste from fiber recycling, for example, deinking sludge that is usually incinerated (Zhang et al., 2015). The combustion residue of paper sludge is PA. The papers reported by Segui et al. (2013) and Onyelowe (2017) demonstrated that PA can provide significant improvement in the geotechnical properties of soil. The use of PA has also shown great potential for the immobilization of both PTEs and organic contaminants from sewage sludge (Pavšič et al., 2014).

Attempts to combine RM with other additives, such as lime (Lee et al., 2011), a combination of lime and zeolite (Friesl et al., 2003), a waste material of the gravel industry (gravel sludge) (Friesl-Hanl et al., 2009), apatite (Shin and Kim, 2016), gypsum (Segui et al., 2013), a combination of water treatment sludge and red gypsum (Gadepalle et al., 2007), coal combustion fly ash (Ciccu et al., 2003), and pulverized fuel ash, shell powder, and Na_2S (Zhang et al., 2019) have been reported.

The objective of this study was to critically valorize neutralized RM from an old disposal site, PA from paper recycling processes, and a mixture of both additives for the remediation of contaminated soil via an immobilization procedure in which a chemically inert geotechnical composite is obtained. The understanding of immobilization mechanisms in such composites is crucial to ensure their environmental compatibility. The goal of this research was to describe those mechanisms on a phenomenological basis. To the best of the authors' knowledge, no cases of soil remediation with PA or with a combination of RM and PA as additives for PTE immobilization are described in the literature. The decision to combine RM with PA in this study was based on the assumption that it would result in improvements in the mechano-physical properties and immobilization effectiveness of the geotechnical composite compared to the case with only RM. Most importantly, it could result in a substantial increase in the RM's recycling potential. The quantity of immobilization additives used in this study (25 wt%) represents a balance between the environmental and physico-mechanical properties of the geotechnical composites employed in the preceding empirical studies in laboratory and practical applications. The implementation of the investigated remediation procedure can provide a large sink for residues from alumina and paper production processes, and, a solution for contaminated soil through the preparation of construction materials with acceptable environmental and mechano-physical performances for usage in geotechnical applications.

The results of this study can represent a basis for more sustainable management and use of the waste materials generated by paper and aluminum industry as well as those generated by the construction sector (e.g. for the rehabilitation of degraded sites). They can initiate the industrial symbiosis in which the closed-loop system is established on a local level.

2. Materials and methods

2.1. Raw materials

Partly neutralized RM obtained from an old depot was a residue of processing of bauxite ore from deposits in the vicinity of Nikšić in Montenegro using the Bayer process at an alumina plant owned by Uniprom-KAP in Podgorica. Approximately 30 kg of RM was sampled from an open disposal site at the alumina plant via the method prescribed in SIST EN 14899 (2006) and dried to a constant mass at 105 °C. According to the European Waste Catalogue (EWC), RM is classified as 01 03 09 (European Commission, 2000). The RM investigated is shown in Fig. S1.

The PA used in this study was generated at a paper mill company, Vipap Videm Krško d.d., located in Krško, Slovenia. It was formed in a steam boiler, in which heat is gained from the incineration of deinking sludge with up to 10 wt% bark. Approximately 90 wt% PA is bottom ash and the remaining 10 wt% is fly ash. According to the EWC, PA is classified as 10 01 01 (European Commission, 2000). A representative sample of approximately 50 kg was collected from a 300-m^3 silo according to the method prescribed in SIST EN 14899 (2006). The sample was stored in a closed, airtight plastic barrel. The PA investigated is shown in Fig. S1.

The contaminated soil (CS) was collected from one of the largest, most degraded areas in Slovenia—the Old Zinc-works site (Fig. S1). This is a degraded site located in the town of Celje with an area of 17 ha. The first zinc ore smelter was established at this historical industrial site in 1873 and was later expanded to include various branches of the metallurgical–chemical industry until all industrial activities in the region ceased in 1990. During all these y of production, the industrial wastes, which mainly consisted of metallurgical slags, ashes, tars, and the tailings of zinc ores, were disposed of or mixed with natural ground on the site itself (Grilc, 2013). The results of chemical analyses of the soil excavated during earthworks at this degraded site classified the soil as hazardous waste (classified as 17 05 03* according to EWC) (European Commission, 2000). Sampling of the CS was performed according to the method prescribed in SIST EN 14899 (2006). In the laboratory, all of the collected material was merged into one representative sample, which was passed through a sieve of 16-mm mesh size. The oversized particles were then crushed in a jaw crusher and mixed with the rest of the sample.

The Brunauer, Emmett, and Teller specific surface area (BETssa) of raw materials was determined by nitrogen gas sorption using ASAP 2020 equipment (Micromeritics, Norcross, Georgia, USA). The density of raw materials was determined using the pyknometer method, according to SIST EN 1097-7 (2008). Their particle-size distribution was determined according to SIST EN 933-1 (2012) and by laser diffraction analysis (particles < 400 μm) using a CILAS 920 Particle Size Analyser (Cilas, Orléans, France).

A total elemental composition analysis of raw materials was performed on powdered samples by a Niton XL 3t GOLDD 900 handheld X-ray fluorescence (XRF) analyzer (Thermo Fisher Scientific Inc., Waltham, Massachusetts, USA) and triplicated. The measurement uncertainty was better than ±5%, with the exception of low As and Hg and high Ti and Ba contents. Leaching tests of raw materials were performed according to SIST EN 12457-2 (2004). The ratio of dry mass of raw material samples to the volume of leaching solution was 1/10. Determination of the contents of Cl^- and SO_4^{2-} in the leachates was performed by UV/Vis spectrophotometry (on a HACH DR/2010 Portable Datalogging Spectrophotometer, Loveland, CO, USA). The measurement uncertainty for the spectrophotometry was ±5%. The contents of As, Ba, Cd, Cr, Cu, Hg, Mo, Ni, Pb, Sb, Se, and Zn were determined in accordance with SIST

EN ISO 17294-2 (2005) using ICP-MS (Agilent 7700x, Agilent Technologies, Tokyo, Japan). The measurement uncertainty of these measurements was better than ±2%. The accuracy of the spectrophotometric determination of Cl^- and SO_4^{2-} was verified by analyzing the standard reference material Anions − Whole Volume (Merck KGaA, Darmstadt, Germany), while the accuracy of the ICP-MS analysis was verified by the determination of elements in standard reference material SPS-SW1 − Reference Material for Measurements of Elements in Surface Waters (Spectrapure Standards, Oslo, Norway). Data are presented in the Supplementary Material (Tables S2 and S3). Good agreement between the determined and certified values was obtained (better than ± 5% for spectrophotometry and better than ± 2% for ICP-MS), confirming the accuracy of the analytical procedure applied.

Mineral phases in the raw materials were characterized by X-ray powder diffraction (XRD), using an Empyrean (PANalytical, Netherlands) diffractometer with Cu−Kα radiation. Powder diffraction data were collected at a tube tension of 40 kV and a tube current of 45 mA using a 2θ step size of 0.02° and measurement time of 100 s per step. The results were analyzed by Highscore (PANalytical, Netherlands) diffraction software, using the Powder Diffraction File PDF-4+ (ICDD, USA) database as the reference source of data. The microstructural and mineralogical features of the raw materials were investigated further by scanning electron microscopy (SEM) using a JEOL 5500 LV (Tokyo, Japan) microscope equipped with energy dispersive spectroscopy (EDS) capability (Oxford Instruments, UK).

To investigate the potential (latent) hydraulic reactivity of the RM and PA samples, pastes made from RM, PA, and a combination of RM and PA were prepared by blending them with an excess of demineralized water (Table 1) in a mortar mixer and curing them for 7, 28, and 56 d in a climatic chamber (at 90% RH and 22 °C). XRD analyses of the pastes as well as SEM/EDS analyses were performed at each curing time interval.

2.2. The investigated geotechnical composites

There were three geotechnical composites investigated in this study, which were prepared by mixing the CS with an additive in a set of selected ratios as shown in Table 2.

The quantity of additives was determined based on empirical data from previous laboratory trials and practical field applications.

Homogenization of geotechnical composites was performed in a planetary blender (Gostol 171, Gostol Nova Gorica, Slovenia) at a speed of 300 rpm for a duration of 5 min. The Modified Proctor Compaction Test (SIST EN 13286−2:2010/AC:2013) was performed to determine their maximum reference dry density (Table S4) and optimum water content (OWC) (Table 2) by using a Proctor compaction device (Automatischer Proctor Type AP, Strassentest, Germany). The determination of the maximum density according to the Proctor Compaction Test can vary by up to ±0.1 Mg/m^3. The test was conducted in a cylindrical mold, A (diameter: 100 mm; height: 120 mm; volume: 942 cm^3), with a rammer, B (4.5 kg), and a compacting energy of 2.66 MJ/m^3. Compaction was performed in five layers, where 25 blows were delivered to each layer with the rammer. This test simulates the field conditions when geotechnical composite is installed in the layers through compaction with heavy rollers. The specimens were removed from the mold by a press and then cured in a climatic chamber at 20 °C and 98% humidity for 3, 7, 28, and 56 d. In total, 15 specimens were prepared for each geotechnical composite.

XRD analysis of the geotechnical composites was performed at each curing time interval. To monitor the formation of crystalline reaction products in the geotechnical composites over time, the relative mass fraction of the newly formed phases was defined by using the reference intensity ratio (RIR) method (I/I_c). Ettringite—one of the most important mineral phases for the chemical immobilization of PTEs (Chen et al., 2009) and the only newly formed crystalline phase detected by XRD—was used as an indicative phase for the relative quantification of the newly formed mineral phases.

The standardized leaching procedure according to SIST EN 1744-3 (2002) was applied to monolithic samples of the geotechnical composites after 7, 28, and 56 d of curing. It was performed using demineralized water as a leaching solution. The leachates were analyzed by ICP-MS and UV−Vis spectrophotometry.

The water permeability of the geotechnical composites was determined after 28 d of curing, whereas their unconfined compressive strength (UCS) was investigated after 3, 7, 28, and 56 d of curing (SIST-TS CEN ISO/TS 17892−11:2004). The measurement uncertainty of the UCS analysis is ±1.5%.

Table 1
Composition of the pastes.

Designation of the pastes	Mixing proportion ratio (wt.%)		
	RM	PA	RM/PA
Red mud	50	0	25
Paper ash	0	50	25
Water	50	50	50

Table 2
Mixing proportions of the investigated geotechnical composites and their designations.

Designation of the composites	Mixing ratios (wt.%)		
	CS/RM	CS/PA	CS/RMPA
Red mud	21.5	0	11.3
Paper ash	0	21.6	10.4
Contaminated soil	64.6	64.9	65.1
Optimum water content	13.9	13.5	13.3

3. Results and discussion

3.1. Raw materials

3.1.1. Red mud

As shown in Table 3, relatively large BETssa and density values were obtained for RM. From the particle-size distribution data (Fig. S2), it is apparent that the median particle size (d_{50}) was smaller than 500 μm.

According to the XRF total elemental analysis (Table S5), the most abundant elements are Ca, Fe, Al, Si, and Ti, followed by an array of minor constituents, including PTEs, such as As, Ba, Cr, Cu, Ni, Pb, and Zn, which are present in the RM in relatively high total concentrations. Based on the leaching test results, it can be concluded that these PTEs are present in the form of low water-soluble species. Only the concentration of Cu exceeded the

Table 3
Surface area (BETssa) and density of the investigated RM, PA, and CS and the basic parameters (pH, conductivity) of their leachates.

Parameter	RM	PA	CS
BETssa (m^2/g)	20.1	8.1	10.0
Density (Mg/m^3)	3.07	2.63	2.71
pH	9.0	12.7	7.5
Conductivity (mS/cm)	0.3	9.7	1.4

Table 4
Concentrations of elements in leachates from RM, PA, and CS with the limiting values for inert materials set by current legislation (Official Gazette of RS, 2018).

Parameter (mg/kg dry matter)	RM	PA	CS	Limiting value for inert materials
SO_4^{2-}	100	20	10,011	6,000
Cl^-	280	120	37	800
As	0.49	<0.01	0.05	0.5
Ba	<0.01	34.9	0.8	20
Cd	<0.01	<0.01	0.34	0.04
Cr	0.03	0.02	<0.01	0.5
Cu	2.2	0.15	0.08	2
Hg	<0.01	<0.01	<0.01	0.01
Mo	0.31	0.06	0.11	0.5
Ni	0.06	<0.01	0.03	0.4
Pb	0.01	0.09	0.48	0.5
Sb	<0.01	<0.01	0.01	0.06
Se	0.02	<0.01	<0.01	0.1
Zn	0.10	0.63	22.61	4

limiting value for inert materials (Table 4).

The concentration of As is also close to the legislation limits, whereas those of all the other elements are far below their limiting values for inertness. This indicates that the investigated RM is a non-hazardous waste material. The results of pH measurements of the leachates (Table 3) indicate that the alkalinity of the investigated RM was partly neutralized by its exposure to atmospheric conditions in an open depot.

The major mineral phases identified in the RM (Fig. 1) were calcite, hematite, and gibbsite, followed by boehmite and a phase that belongs to the feldspathoid group of minerals (cancrinite/vishnevite). Goethite, quartz, ilmenite, illite/muscovite, perovskite, and rutile are present as minor constituents. The results of the SEM/EDS analysis further revealed the presence of dolomite as a minor mineral phase of the RM. On the basis of the EDS analysis, the mineral phase from the feldspathoid group was determined to be cancrinite (Fig. S3). No reactive mineral phases, such as one of the principal mineralogical constituents of RM from the sintering process, dicalcium silicate (Sutar et al., 2014), were identified in the RM.

The results of the XRD analysis (Fig. S4) together with the SEM/EDS analysis of the RM paste indicate that the RM is not a hydraulically active material as no new mineral phases (reaction products) were formed during the different curing time intervals.

3.1.2. Paper ash

PA is a fine-grade material with a d_{50} value of 89 μm (Fig. S2).

The data of the total element concentrations (Table S5) showed that Ca is the most abundant element, together with Si, Al, and Mg. The less abundant elements are Ba, Fe, S, and K, followed by Zn and Ni. There are also other elements present in trace amounts.

The leaching test (Table 4) showed that the water soluble concentration of Ba was 1.7 times higher than the limiting value for inert materials. None of the other PTE exceeded the values for inertness set by the legislation (Official Gazette of RS, 2018), so the PA should be regarded as non-hazardous waste.

Calcite represented the major crystalline phase, along with lime and portlandite. Quartz, talc, gehlenite, anhydrite, and dolomite are mineral phases that occur as minor phases (Fig. 2). The elevated background in the XRD spectra reflects the presence of an amorphous phase. The presence of high concentrations of water-soluble lime and portlandite is the reason for the high alkalinity of the PA leachate.

The presence of an amorphous phase was further confirmed by the SEM/EDS analysis. The phase occurs in various irregularly shaped grains made of a vitreous groundmass with small rounded pores (Fig. S5). The EDS analysis revealed that the amorphous phase consists mainly of Si, Al, and Ca. The associated minor elements are K, Na, Mg, Cl, and Fe in different proportions. The phase consisting of Ba and S was also identified by SEM/EDS.

The results of the XRD analysis of the PA paste (Fig. 3) showed that, after 7 d, different calcium aluminate hydrates (CAH) were formed: hemicarboaluminate (Hc), hydrocalumite (Hy), and monocarboaluminate (Mc). A clear transition of Hc to Mc was observed at longer curing time intervals. The results confirmed that the PA is hydraulically active.

The results of the SEM/EDS analysis further confirmed the

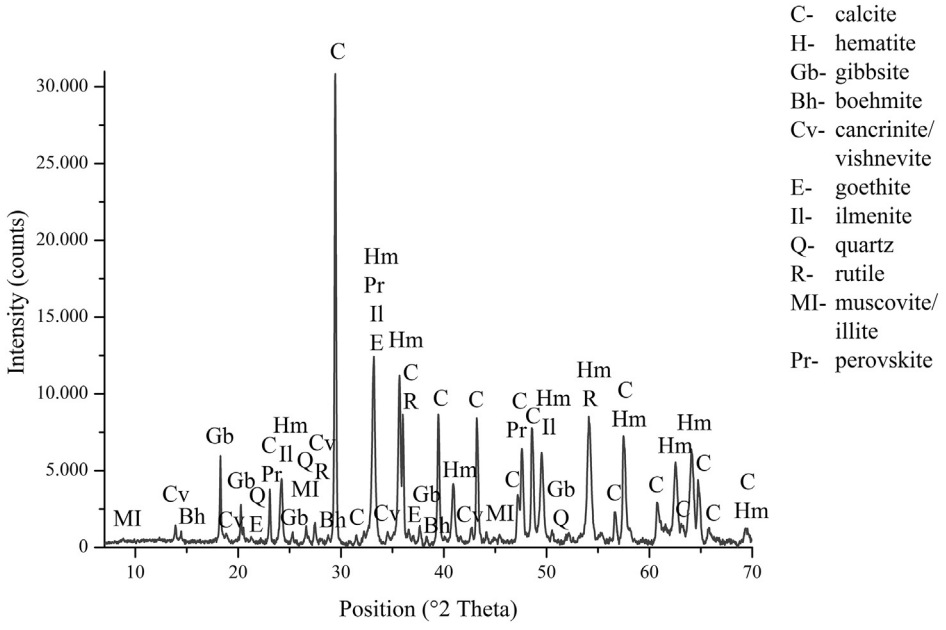

Fig. 1. XRD pattern of the RM.

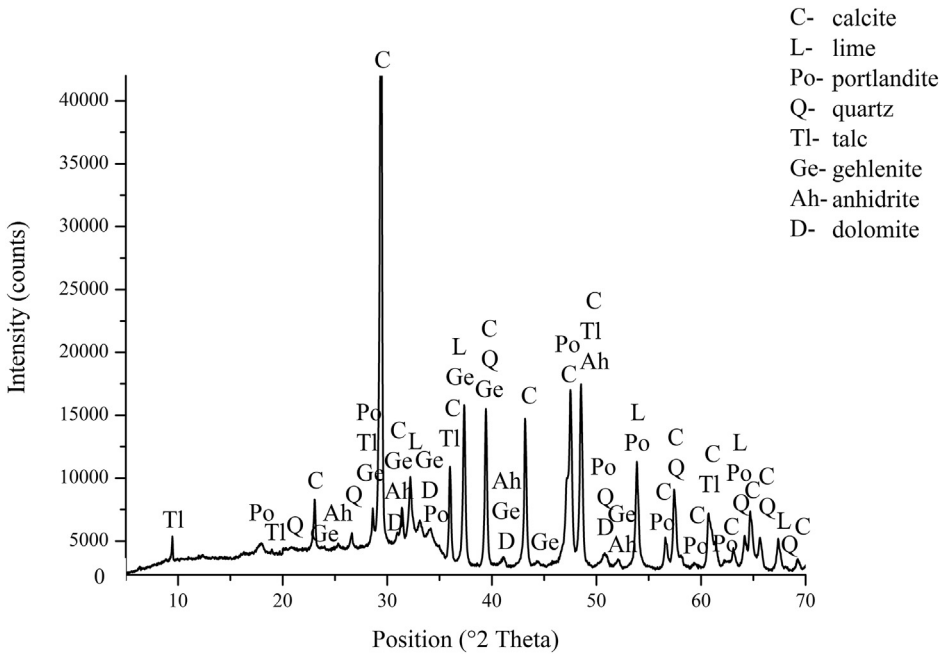

Fig. 2. XRD pattern of the PA.

hydraulic activity of the PA, because of the generation of reaction rims around the amorphous phase grains in the groundmass of the PA paste (Fig. S6).

After 7 d of curing, two different CAH phases were formed in PA and RM/PA pastes: Hc and Mc. At longer curing time intervals, a marginal depletion of Hc was observed, but its transformation into Mc was not significant, notwithstanding the excess calcite in the RM/PA paste on account of the presence of PA. In comparison to the PA paste, the relative quantity of CAH formed in the RM/PA paste was smaller by a factor of more than two. This leads to the conclusion that the RM could not be activated by lime or portlandite from the PA, which confirms the finding that the investigated RM is not a (latent) hydraulic material. The results of the SEM/EDS analysis of the RM/PA paste revealed partially reacted grains of PA, whereas on the fragments of RM, no evidence of the reaction could be identified (Fig. S7).

3.1.3. Contaminated soil

The total concentrations of As, Cd, Cu, Hg, Ni, Pb, and Zn (Table S5) exceeded the critical limit values set by Slovenia's national Soil Quality Decree (Official Gazette of RS, 1996). The most critical parameters in the CS leachate (Table 4) were Pb, Cd, Zn, and sulfate concentrations. Cd, Zn, and sulfate exceeded the limiting values for inertness.

Fig. 4 presents the results of the mineralogical analysis. Quartz, dolomite, calcite, muscovite/illite, anorthite, and chlorite are presumably the phases from the geological ground, whereas gypsum, gahnite, franklinite, mullite, hemimorphite, hematite, cerussite, zincite, and goslarite are mineral phases that presumably originate from the slag fragments and other metallurgical-chemical waste in the CS.

Franklinite and gahnite are the primary Zn-bearing mineral phases in the metallurgical slag. As members of the spinel group,

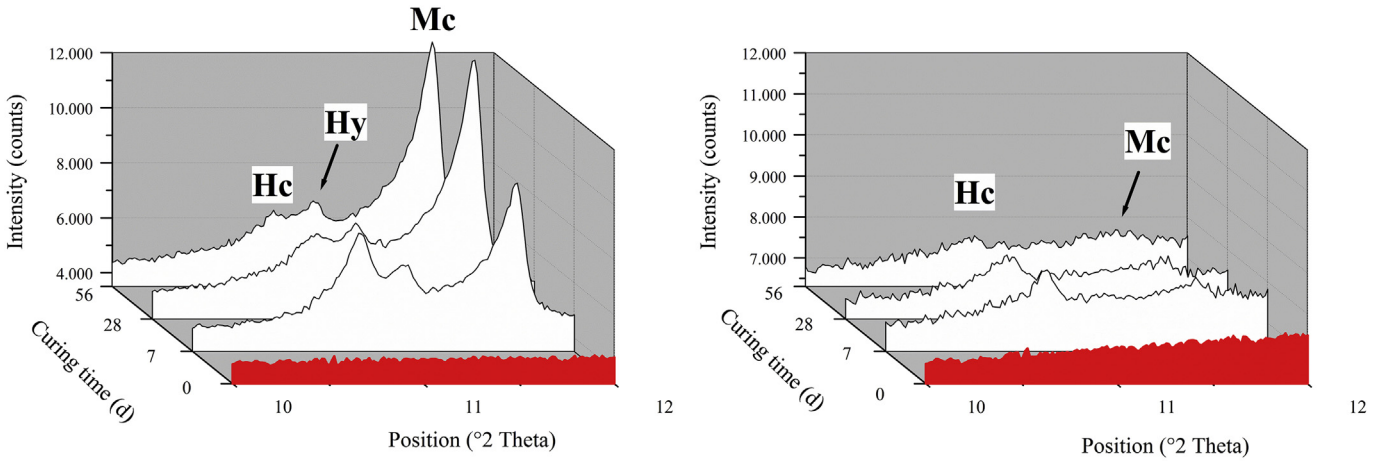

Fig. 3. Sections of the XRD patterns of the PA (left) and RM/PA (right) pastes. The most intense peaks of the newly formed mineral phases, hemicarboaluminate (Hc), hydrocalumite (Hy), and monocarboaluminate (Mc), are indicated.

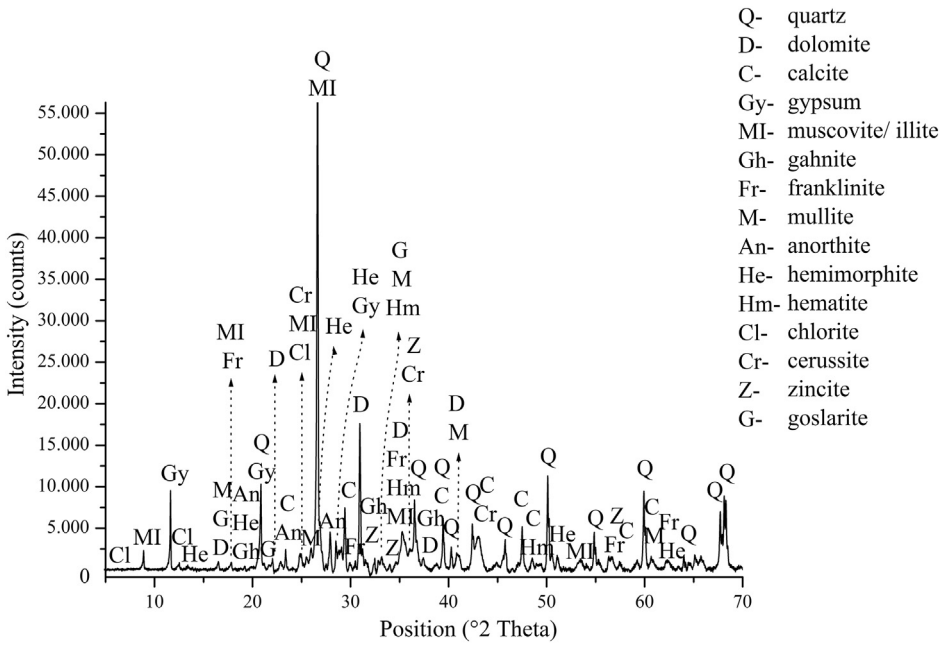

Fig. 4. XRD pattern of CS.

these two phases are considered to be highly stable. Pb was mostly found in its elemental and oxide forms. Secondary minerals were formed after the weathering of primary minerals of the slag. Cerussite, gypsum, goslarite, and zincite were determined in the CS by XRD, and mimetite was determined by SEM/EDS. These minerals are highly susceptible to dissolution (Vanaecker et al., 2014) and represent the most probable source of Zn, Pb, and SO_4^{2-} in the leaching tests. The mineralogical compositions of the metallurgical slags from the CS are similar to those reported by various authors who have investigated sites contaminated by zinc and lead smelting processes (Vanaecker et al., 2014).

3.2. Investigated geotechnical composites

3.2.1. Mineralogical composition

In the CS/RM geotechnical composite, no newly formed reaction products were identified (Fig. S8). Ettringite was identified in the CS/PA and CS/RMPA already after 7 d (Fig. 5).

The formation of ettringite was attributed to the reaction of the latent hydraulic active mineral phases from the PA with sulfate from the CS. The amorphous phase of the PA started to dissolve when brought into contact with alkaline pore solution, which resulted from dissolution of portlandite. As soluble sulfate in the form of gypsum was also present in the system, ettringite was formed. Sulfate consumption and dissolution of the amorphous phase progressed gradually over time, which was reflected in an increase in the relative quantity of ettringite in the composites.

The progress of ettringite formation (Fig. 6) in CS/RMPA over time is similar to that in the CS/PA composite, but the relative quantities differ significantly.

Reaction products of CS/PA and CS/RMPA were further identified by an SEM/EDS analysis. In Fig. S9, the CAH phase incorporating sulfate is shown, where the typical microstructure of ettringite, described as “tiger stripe” morphology (Diamond, 2004), can be seen.

3.2.2. Immobilization efficiency and environmental assessment

All concentrations of PTEs in the leachates from the CS/RM were below the limiting values for inert materials (Table S6, Fig. 7) (Official Gazette of RS, 2018).

The mechanisms of PTE immobilization by RM are governed by

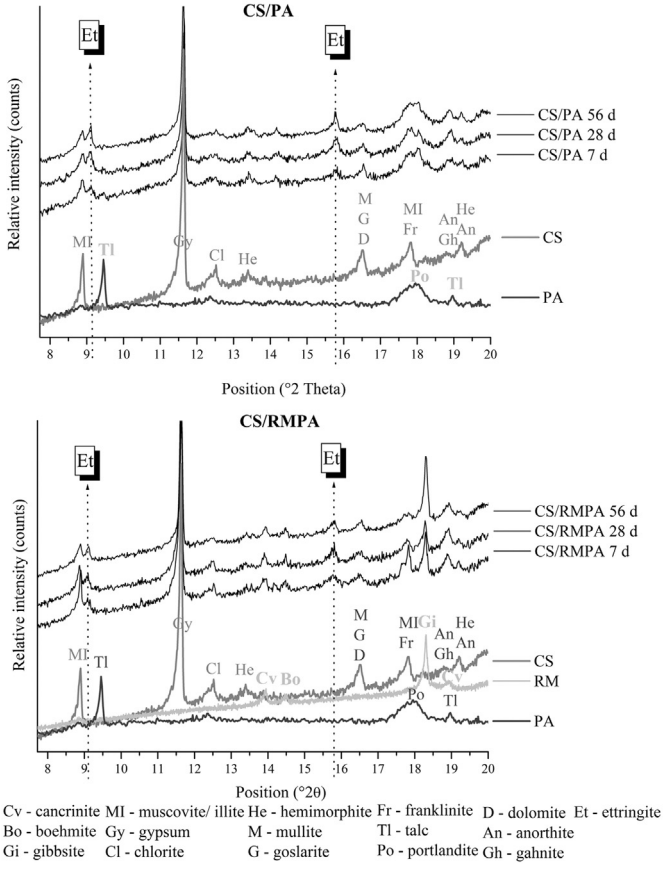

Fig. 5. Sections of the XRD patterns of CS/PA and CS/RMPA, along with the XRD patterns of the materials used. The two main peaks corresponding to ettringite (Et) are indicated by dotted lines.

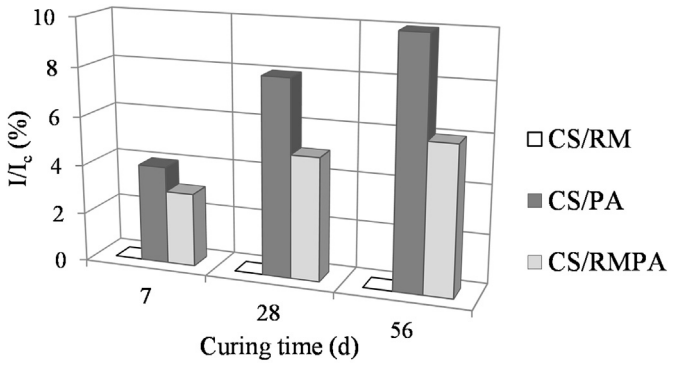

Fig. 6. Relative mass fraction of ettringite formed in CS/RM, CS/PA, and CS/RMPA after different curing intervals.

surface sorption and precipitation processes (Liu et al., 2011). The constituents of RM, which provide a large number of adsorption sites due to their high specific surface area, are the iron and aluminum hydroxide mineral phases, goethite, hematite, the feldspathoid group of minerals, and gibbsite.

The pH of the RM is favorable for immobilization as it is close to the neutral value, where multiple PTEs have their adsorption maxima (Pichinelli et al., 2017). No time-dependent trends in the immobilization efficiency could be defined for most of the PTEs as their adsorption is a relatively fast process. A minor time-dependent increase in the immobilization of Cd, Pb, and Zn was observed nevertheless. This could be attributed to the slow diffusion of ions of those PTEs in the composite before they had reached the adsorption sites. There was a minor increase in the concentrations of As and Mo in the leachates from CS/RM compared to the leachates from CS, which can be attributed to the discharge of these elements from RM, as reported in the literature (Hua et al., 2017). Another reason is that oxyanions are mobile and less efficiently adsorbed at the pH level of CS/RM.

The absence of cations that could form low-soluble complexes with sulfate limited the latter's immobilization in CS/RM compared to the other composites (Fig. 8).

Sulfate anions cannot be adsorbed onto the surface adsorption sites of RM particles because they are negatively charged at the pH level of CS/RM (Fig. 9). This is in agreement with the surface complexation models (Dzombak and Morel, 1990). Nevertheless, sulfate in CS/RM was successfully immobilized below the limiting values for inertness. The most alkaline leachate, with pH 11.5, was measured in the case of CS/PA (Fig. 9).

The lowering of pH and conductivity in the leachates from CS/PA followed a time-dependent trend. This was attributed to the gradual formation of reaction mineral products that consumed dissolved ions and the neutralized alkalinity of the pore solution (Fernández et al., 2010; Garrabrants and Kosson, 2005). Lower concentrations of As were determined in the leachates from CS/PA compared to CS/RM (Table S6), despite the former having a higher pH value, which usually favors the mobilization of As(V) and As(III) oxyanions. The successful immobilization of As which occurred in CS/PA was attributed to the formation of $Ca_3(AsO_4)_2 \times 3{-}10H_2O$ and/or the incorporation of these oxyanions in the CAH phases (Chen et al., 2009). Compared to the Cd and Zn in CS/RM, Cd and Zn in the leachates from CS/PA were present in lower concentrations. High pH values favored the formation of low-solubility $Cd(OH)_2$ and $CaCd(OH)_4$ and the immobilization of Cd in the newly formed reaction products (Malviya and Chaudhary, 2006). A possible chemical immobilization mechanism of Zn is the formation of low-soluble phases, such as calcium hydroxyzincate

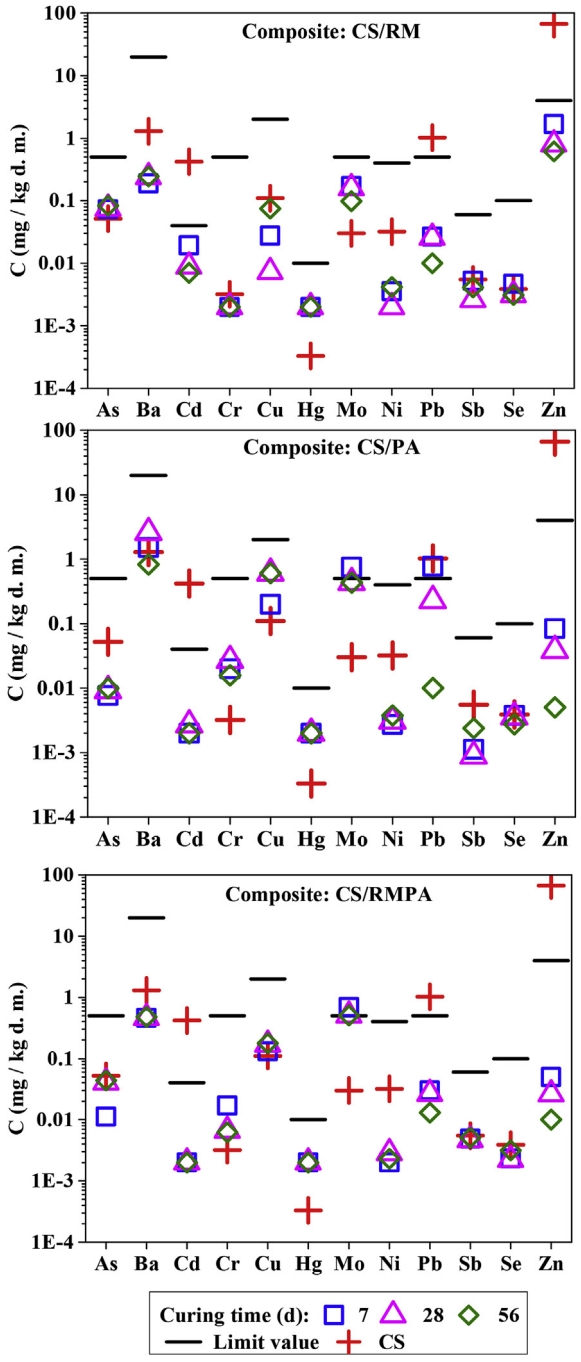

Fig. 7. Concentrations of PTEs in the leachates from CS/RM, CS/PA, CS/RMPA, and CS. The limiting values for inertness correspond to the values permitted by the landfilling regulation (Official Gazette of RS, 2018).

($CaZn_2(OH)_6 \times 2H_2O$) and zinc hydroxide (Mellado et al., 2013). This is in agreement with the time-dependent trend in the lowering of Zn concentrations due to the gradual formation of reaction products with longer curing times. Alkaline pH values resulted in less efficient immobilization of Cr and Mo oxyanions, Cu, and Pb (Kogbara et al., 2014). The concentrations of Cr and Cu in CS were already well below the limiting values for inert materials. There is a clear time-dependent trend in the lowering of Mo and Pb concentrations below the prescribed inertness limits. The immobilization of Mo was attributed to the formation of $CaMoO_4$ and to its incorporation in the CAH phases (Cornelis et al., 2008). The

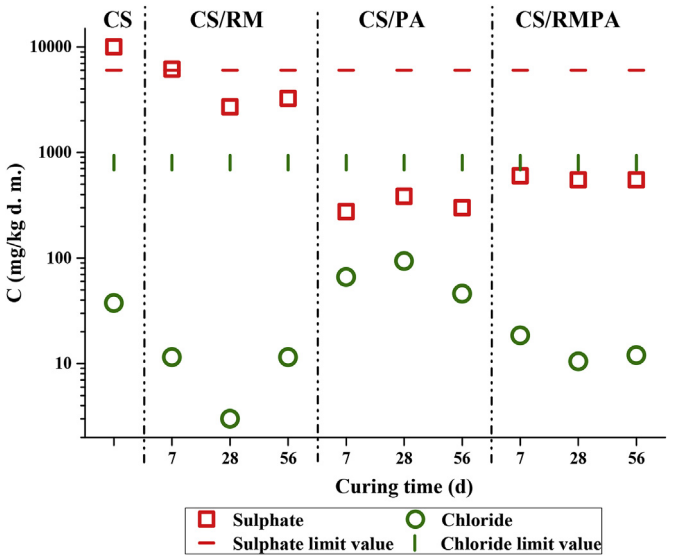

Fig. 8. Leaching of sulfate and chloride from CS/RM, CS/PA, CS/RMPA, and CS. The limiting values for inertness correspond to the values permitted by the landfilling regulation (Official Gazette of RS, 2018).

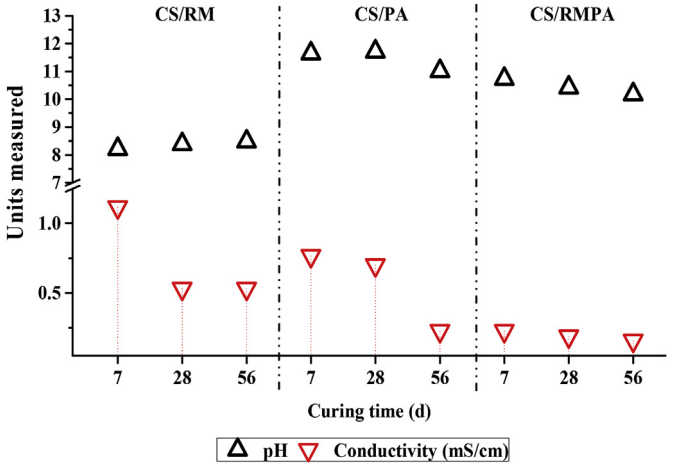

Fig. 9. pH and conductivity of the leachates from CS/RM, CS/PA, and CS/RMPA.

immobilization of Pb was due to its incorporation in the newly formed minerals and co-precipitation (Chen et al., 2009). The concentrations of Ba were highest in the leachates from CS/PA compared to the other two composites. This was attributed to Ba's leaching from PA. In CS/PA, the immobilization of Ba was controlled by the precipitation of low-soluble $BaSO_4$ (Cappuyns, 2018), which consumed the soluble sulfate from CS. This soluble sulfate was also consumed partly due to the formation of ettringite. After 28 d of curing of CS/PA, all the PTEs were below the limiting values for inertness.

The immobilization of PTE was not as efficient in CS/RMPA as in SC/RM. The time-dependent trends for the immobilization of Mo, Pb, and Zn were less pronounced but still observable. In CS/RMPA, the concentration of Ba was twice as high and sulfate leaching was 5–10 times lower than in the case of CS/RM. This was attributed both to the use of PA, which caused the release of Ba, and to the formation of $BaSO_4$, $CaSO_4$, and ettringite. All the parameters, except for the Mo concentration, were below the limiting values for inert materials in the leachates. Due to a combination of less

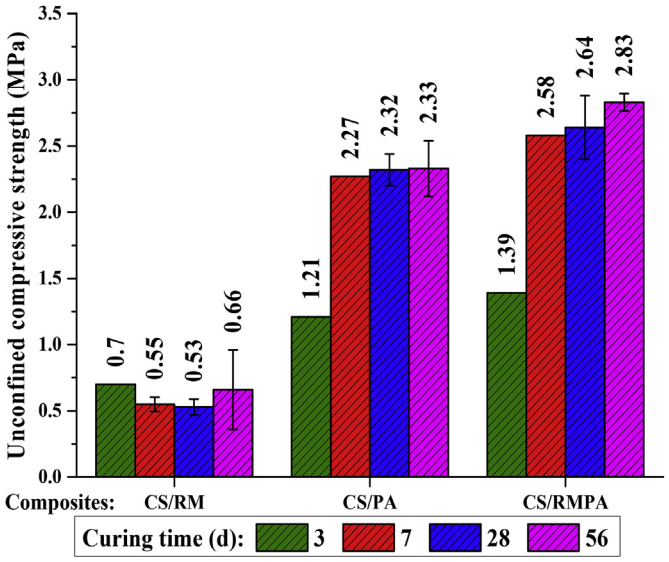

Fig. 10. Development of the UCS in the case of CS/RM, CS/PA, and CS/RMPA.

efficient immobilization and alkaline pH values of CS/RMPA composite (Fig. 9), the solubility of molybdate and other oxyanion species from CS and the aluminum solubility from RM may be increased (Milačič et al., 2012). Their potential leaching from CS/RMPA composite may represent a limiting factor in environmental acceptability of composites with addition of RM.

3.2.3. Mechano-physical characteristics

There were only minor differences between the geotechnical composites regarding the optimum water content (OWC) (Table 2, Fig. S10). For instance, the consumption of water at OWC needed to achieve the desired maximum compaction was, in the case of the CS/RM, governed by the RM's high specific surface area. The CS/PA consumed water mainly on account of the exothermic reaction between the free lime from PA and water. When compared to data given in the literature, the OWC values for CS/PA obtained in this study were lower than those reported elsewhere (Segui et al., 2013), mainly due to the variations in the characteristics of the raw materials used.

The lowest values of UCS were measured in the case of CS/RM (Fig. 10). This is in agreement with the finding that no new mineral phases that could contribute to the binding of the composite were formed. Both CS/PA and CS/RMPA had a UCS that was almost twice as high as that of CS/RM after 3 d of curing. After 56 d, the UCS values were 3.3 times higher in the case of CS/PA and 4 times higher in the case of CS/RMPA. These increases were due to the formation of new hydraulic reaction products as the duration of the curing period increased.

The most pronounced increase in the UCS of CS/PA and CS/RMPA was observed during the early ages of curing, that is, between 3 and 7 d. Similar observations with the use of PA were reported by Segui et al. (2013). Although more reaction products were formed in CS/PA than in CS/RMPA, an approximately 1.2 times higher UCS was measured in the case of CS/RMPA. This is attributed to the physical properties of the RM, which acted as a filler to support the grains more efficiently. According to Slovenian Technical Specifications (DARS, 2001), CS/PA (after 56 d of curing) and CS/RMPA (after 7 d of curing) comply with the UCS limit values (>2.5 MPa) for use as a base course for roads.

The water permeability values of CS/RM, CS/PA, and CS/RMPA were 7.88×10^{-8}, 3.97×10^{-9}, and 5.19×10^{-8} m/s. Despite the

lower content of fine grains in CS/PA compared to CS/RMPA and CS/RM, the hydraulic conductivity of the former was the lowest. This indicates that the formation of new mineral phases, which are present in the largest quantities in CS/PA, not only contributes to the UCS of the composite but also affects the water permeability due to the pore filling effect.

The higher concentrations of As, Cd, Zn, and SO_4^{2-} in the leachates from CS/RM (Figs. 7 and 8) can be correlated with this composite's higher water permeability compared to CS/PA and CS/RMPA. The low water permeability of CS/PA does not increase the immobilization efficiency for all PTEs, although the differences are small. This suggests that leaching from CS/PA is also driven by a diffusion mechanism. The latter depends on the concentration gradient between the demineralized water as a leaching solution and the concentrated pore solution with dissolved PTE species (Garrabrants and Kosson, 2005).

4. Conclusions

The potential use of large quantities of red mud, paper ash, and a combination of both additives in the production of inert construction products—geotechnical composites from contaminated soil—was proved to be possible in this study. It was shown that neutralized RM from an old depot can be used in relatively high quantities as an additive for the immobilization of CS to produce inert geotechnical composite. The extent of leaching of SO_4^{2-}, Zn, Pb, and Cd from the CS/RM composite, in comparison to CS, was more than 3, 37, 48, and 34 times lower. The potential use of CS/RM composite is limited to applications where high mechano-physical properties are not required.

It was also shown that PA can be used for the production of inert geotechnical composite from CS. In comparison to CS itself, the extent of leaching of SO_4^{2-} from the CS/PA composite was more than 33 times lower, while the leaching of Zn, Pb, and Cd was lowered for more than 2260, 48, and 34 times. The concentration of Mo in the leachates from CS/PA decreased with curing time, and was, after 28 d, measured to be below the limiting values. On account of the hydraulic properties of PA, its use as an additive resulted in the formation of the composite with the lowest water-permeability characteristics and good mechanical properties. These properties are very favorable for the use of the CS/PA composite in the construction sector and for the microencapsulation of various PTEs within a low-water-permeable matrix.

The use of a combination of RM and PA for the production of the CS/RMPA geotechnical composite has been investigated for the first time. In comparison to CS, the concentration of SO_4^{2-} in the leachate from CS/RMPA composite was more than 18 times lower, while the concentrations of Zn were similar to those seen in the CS/PA composite. The efficiency of immobilization of Pb and Cd in the CS/RMPA composite was comparable to that in the CS/RM and CS/PA composites. Similarly to the concentration of Mo in the leachates from CS/RM and CS/PA, the concentration of Mo in the leachate from CS/RMPA decreased with curing time, but after 28 d and 56 d, it slightly exceeded the limiting value for inertness. The highest compressive strength was measured in the case of CS/RMPA composite, which implies that the combination of RM and PA results in improved mechano-physical properties of the geotechnical composites compared to the use of RM only.

Further research will be targeted towards tailoring the application rates of RM and PA to the characteristics of a specific contaminated soil. The potential improvement of the CS/RMPA composite with additional additives will be tested and optimized to achieve successful immobilization of molybdate and other oxyanions. The applicability of such construction composites will be investigated for construction purposes where large quantities of materials are needed e.g. rehabilitation of exploited mining areas in the case of CS/RM, construction of stabile dams for safe storage of industrial and mining waste in the case of composites with PA. Red mud is increasingly considered as a source for extraction of valuable elements (such as rare earth elements), therefore the use of extraction residues for the purpose of soil remediation as described in this study will also be the focus of future studies.

The described application of waste materials generated by alumina and paper production processes for the remediation of contaminated soil is in line with the principles of sustainable material design, which leads to closed-loop material cycles. The remediation procedure investigated can provide a basis for establishing an industrial symbiosis between the aluminum, paper and construction sectors. Such a symbiosis can lead to the mitigation of environmental impacts related to the alleviation of the landfilling burden, lowering of emissions, preservation of natural materials, reduction of health risks related to soil contamination and, ultimately, to a more self-sufficient society.

Author contribution

P. Oprčkal: Conceived and designed the analysis, Collected the data, Contributed data or analysis tools, Performed the analysis; Wrote the paper; A. Mladenovič: Conceived and designed the analysis, Collected the data, Contributed data or analysis tools, Wrote the paper; N. Zupančič: Contributed data or analysis tools, Performed the analysis, Wrote the paper; J. Ščančar; Conceived and designed the analysis; Contributed data or analysis tools, Performed the analysis, Wrote the paper; R. Milačič: Conceived and designed the analysis, Contributed data or analysis tools, Performed the analysis, Wrote the paper; V. Zalar Serjun: Conceived and designed the analysis, Collected the data, Contributed data or analysis tools, Performed the analysis, Wrote the paper

Declaration of competing interest

The authors declare that they have no known competing financial interests or personal relationships that could have appeared to influence the work reported in this paper.

Acknowledgments

The authors acknowledge the Slovenian Research Agency - core fundings P2-0273, P1-0143, V1-1649, L7-6747, J1-7148, L1-9190, and Z1-1858. The authors would like to thank Assistant Professor Dr Irena Nikolić from the University of Montenegro (Faculty of Metallurgy and Technology) for providing the red mud samples.

Appendix A. Supplementary data

Supplementary data to this article can be found online at https://doi.org/10.1016/j.jclepro.2020.120440.

References

Cappuyns, V., 2018. Barium (Ba) leaching from soils and certified reference materials. Appl. Geochem. 88 (part A), 68–84. https://doi.org/10.1016/j.apgeochem.2017.05.002.

Chen, Q.Y., et al., 2009. Immobilisation of heavy metal in cement-based solidification/stabilisation: a review. Waste Manag. 29 (1), 390–403. https://doi.org/10.1016/j.wasman.2008.01.019.

Ciccu, R., et al., 2003. Heavy metal immobilization in the mining-contaminated soils using various industrial wastes. Miner. Eng. 16, 187–192. https://doi.org/10.1016/S0892-6875(03)00003-7.

Cornelis, G., et al., 2008. Leaching mechanisms of oxyanionic metalloid and metal species in alkaline solid wastes: a review. Appl. Geochem. 23 (5), 955–976. https://doi.org/10.1016/j.apgeochem.2008.02.001.

DARS [Motorway Company in the Republic of Slovenia], 2001. TSC 06.320 : 2001

Vezane Spodnje Nosilne Plasti S Hidravličnimi Vezivi [Bonded Materials for Base Course Road Foundation with Hydraulic Binders]. Slovenski inštitut za standardizacijo (SIST), Ljubljana, 10/2001.
Diamond, S., 2004. The microstructure of cement paste and concrete—a visual primer. Cement Concr. Compos. 26 (8), 919–933. https://doi.org/10.1016/j.cemconcomp.2004.02.028.
Dzombak, D.A., Morel, F.M.M., 1990. Surface Complexation Modeling, Hydrous Ferric Oxide. John Wiley & Sons, Canada.
EEA – European Environmental Agency, 2014. Progress in Management of Contaminated Sites (CSI 015) accessed 20 September 2017. www.eea.europa.eu/data-andmaps/indicators/progress-in-management-ofcontaminated-sites/progress-inmanagement-of-contaminated-1/.
European Commission, 2008. Directive 2008/98/EC of the European Parliament and of the Council of 19 November 2008 on waste and repealing certain directives. Off. J. L 312/3, 22/11/2008.
European Commission, 2006. Integrated Pollution Prevention and Control. Reference Document on Best Available Techniques for the Waste Treatments Industries.
European Commission, 2000. Commission decision replacing decision 94/3/EC establishing a list of wastes pursuant to article 1(a) of council directive 75/442/EEC on waste and council decision 94/904/EC establishing a list of hazardous waste pursuant to article 1(4) of council directive 91/689/EEC on hazardous waste. Off. J. L 226, 6/9/2000.
Fernández, R., et al., 2010. Mineralogical and chemical evolution of hydrated phases in the pozzolanic reaction of calcined paper sludge. Cement Concr. Compos. 32 (10), 775–782. https://doi.org/10.1016/j.cemconcomp.2010.08.003.
Friesl, W., et al., 2003. Immobilisation of heavy metals in soils using inorganic amendments in a greenhouse study. J. Plant Nutr. Soil Sci. 166, 191–196. https://doi.org/10.1002/jpln.200390028.
Friesl-Hanl, W., et al., 2009. Immobilising of Cd, Pb, and Zn contaminated arable soils close to a former Pb/Zn smelter: a field study in Austria over 5 years. Environ. Geochem. Health 31, 581–594. https://doi.org/10.1007/s10653-009-9256-3.
Gadepalle, V.P., Ouki, S.K., Van Herwijnen, R., Hutchings, T., 2007. Immobilization of heavy metals in soil using natural and waste materials for vegetation establishment on contaminated sites. Soil Sediment Contam. 16 (2), 233–251. https://doi.org/10.1080/15320380601169441.
Garrabrants, A.C., Kosson, D.S., 2005. Leaching processes and evaluation tests for inorganic constituent release from cement-based matrices. In: Spence, R.D., Shi, C. (Eds.), Stabilization and Solidification of Hazardous, Radioactive, and Mixed Wastes. CRC Press, MA, USA, pp. 229–280.
Grilc, V., 2013. Priprava onesnaženega zemljišča Stare Cinkarne v Celju na sanacijo. In: Grabne, B., Ribarič Lasnik, C. (Eds.), Environmental Pollution and Natural Resources as a Limiting Factor for Development in Slovenia – Celje Basin as a Model Approach for Degraded Areas. Inštitut Za Okolje in Prostor, Celje, Slovenija, pp. 23–35.
Hua, Y.M., Heal, K.V., Friesl-Hanl, W., 2017. The use of red mud as an immobiliser for metal/metalloid-contaminated soil: a review. J. Hazard Mater. 325, 17–30. https://doi.org/10.1016/j.jhazmat.2016.11.073.
Khairul, M.A., Zanganeh, J., Moghtaderi, B., 2019. The composition, recycling and utilisation of Bayer red mud. Resour. Conserv. Recycl. 141, 483–498. https://doi.org/10.1016/j.resconrec.2018.11.006.
Klauber, C., Gräfe, H., Power, G., 2011. Bauxite residue issues: II. Options for residue utilization. Hydrometallurgy 108, 11–32. https://doi.org/10.1016/j.hydromet.2011.02.007.
Kogbara, R.B., Al-Tabbaa, A., Stegemann, J.A., 2014. Comparisons of operating envelopes for contaminated soil stabilised/solidified with different cementitious binders. Environ. Sci. Pollut. Res. 21 (5), 3395–3414. https://doi.org/10.1007/s11356-013-2276-7.
Lee, S.-H., et al., 2011. In situ stabilization of arsenic and metal-contaminated agricultural soil using industrial by-products. Geoderma 161 (1–2), 1–7. https://doi.org/10.1016/j.geoderma.2010.11.008.
Liu, Y., Naidu, R., Ming, H., 2011. Red mud as an amendment for pollutants in solid and liquid phases. Geoderma 163 (1–2), 1–12. https://doi.org/10.1016/j.geoderma.2011.04.002.
Malviya, R., Chaudhary, R., 2006. Factors affecting hazardous waste solidification/stabilization: a review. J. Hazard Mater. 137 (1), 267–276. https://doi.org/10.1016/j.jhazmat.2006.01.065.
Mellado, A., et al., 2013. Immobilization of Zn(II) in Portland cement pastes. J. Therm. Anal. Calorim. 112 (3), 1377–1389. https://doi.org/10.1007/s10973-012-2705-8.
Official Gazette of, R.S., 2018. Decree on Waste Landfill, Nos. 10/14, 54/15, 36/16, and 37/18.
Milačič, R., Zuliani, T., Ščančar, J., 2012. Environmental impact of toxic elements in red mud studied by fractionation and speciation procedures. Sci. tot. environ. 426, 359–365. https://doi.org/10.1016/j.scitotenv.2012.03.080.
Official Gazette of, R.S., 1996. Decree on Limit Values, Alert Thresholds and Critical Levels of Dangerous Substances into the Soil, No. 68/96. Part of Environmental Protection Act No. 41/04.
Onyelowe, K.C., 2017. Nanostructured waste paper ash treated lateritic soil and its California bearing ratio optimization. Global J. Technol. Optim. 8 (2), 1–6. https://doi.org/10.4172/2229-8711.1000220.
Pavšič, P., et al., 2014. Sewage sludge/biomass ash based products for sustainable construction. J. Clean. Prod. 67, 117–124. https://doi.org/10.1016/j.jclepro.2013.12.034.
Pichinelli, B.C., et al., 2017. Adsorption of Ni(II), Pb(II) and Zn(II) on $Ca(NO_3)_2$-neutralised red mud. Water Air Soil Pollut. 228 (24) https://doi.org/10.1007/s11270-016-3208-1.
Segui, P., et al., 2013. Valorisation of wastepaper sludge ash as main component of hydraulic road binder. Waste Biomass Valoris 4 (2), 297–307. https://doi.org/10.1007/s12649-012-9155-1.
Segui, P., et al., 2012. Characterization of wastepaper sludge ash for its valorization as a component of hydraulic binders. Appl. Clay Sci. 57, 79–85.
Shin, W., Kim, Y.-K., 2016. Stabilization of heavy metal contaminated marine sediments with red mud and apatite composite. J. Soils Sediments 16, 726–735. https://doi.org/10.1007/s11368-015-1279-z.
SIST EN 933-1, 2012. Tests for Geometrical Properties of Aggregates – Part 1: Determination of Particle Size Distribution – Sieving Method.
SIST EN 1097-7, 2008. Tests for Mechanical and Physical Properties of Aggregates – Part 7: Determination of the Particle Density of Filler – Pyknometer Method.
SIST EN 1744-3, 2002. Tests for Chemical Properties of Aggregates – Part 3: Preparation of Eluates by Leaching of Aggregates.
SIST EN 12457-2, 2004. Characterisation of Waste – Leaching – Compliance Test for Leaching of Granular Waste Materials and Sludges. Part 2, One Stage Batch Test at a Liquid to Solid Ratio of 10 L/kg for Materials with Particle Size below 4 Mm (Without or with Size Reduction).
SIST EN 13286-2:2010/AC, 2013. Unbound and Hydraulically Bound Mixtures – Part 2: Test Methods for Laboratory Reference Density and Water Content – Proctor Compaction.
SIST EN 14899, 2006. Characterization of Waste – Sampling of Waste Materials – Framework for the Preparation and Application of a Sampling Plan.
SIST EN ISO 17294-2, 2005. Water Quality – Application of Inductively Coupled Plasma Mass Spectrometry (ICP MS) – Part 2: Determination of 62 Elements.
SIST-TS CEN ISO/TS 17892-11, 2004. Geotechnical Investigation and Testing – Laboratory Testing of Soil – Part 11: Determination of Permeability by Constant and Falling Head. ISO/TS 17892-11: 2004.
Sutar, H., et al., 2014. Progress of red mud utilization: an overview. Am. Chem. Sci. J. 4 (3), 255–279.
Vanaecker, M., et al., 2014. Behavior of Zn-bearing phases in base metal slag from France and Poland: a mineralogical approach for environmental purposes. J. Geochem. Explor. 136, 1–13. https://doi.org/10.1016/j.gexplo.2013.09.001.
van Hees, P.A.W., et al., 2008. Re-cycling of remediated soil in Sweden: an environmental advantage? Resour. Conserv. Recycl. 52 (12), 1349–1361. https://doi.org/10.1016/j.resconrec.2008.07.016.
Zhang, Z., et al., 2019. Amendments for simultaneous stabilization of lead, zinc, and cadmium in smelter-contaminated topsoils. Environ. Eng. Sci. 36 (3), 326–334. https://doi.org/10.1089/ees.2018.0231.
Zhang, Z., et al., 2015. Simultaneous recovery of organic and inorganic content of paper deinking residue through low-temperature microwave-assisted pyrolysis. Environ. Sci. Technol. 49 (4), 2398–2404. https://doi.org/10.1021/es505249w.
Zhou, Y.-F., Haynes, R.J., 2010. Sorption of heavy metals by inorganic and organic components of solid wastes: significance to use of wastes as low-cost adsorbents and immobilizing agents. Crit. Rev. Environ. Sci. Technol. 40 (11), 909–977. https://doi.org/10.1080/10643380802586857.